Non-Decoupling Dark Matter

MING-SHAU LIU
CAVENDISH LABORATORY,
UNIVERSITY OF CAMBRIDGE

SUPERVISER:
DR TEVONG YOU AND DR JIM TALBERT

The preliminary study of this work is carried out as part of the
CERN Non-Member State Summer Student Programme 2022
The extension is carried out as the Research Project for
Part III Natural Science Tripos at the University of Cambridge 2023

Submitted, May 2023

NON-DECOUPLING DARK MATTER

Candidate Number: 8224X
Supervisor: Dr Tevong You and Dr Jim Talbert

ABSTRACT: We study non-composite dark matter as a beyond the Standard Model (BSM) extension under the Higgs Effective Field Theory (HEFT) framework, which describes necessarily non-linearly realised theories perturbed around the ground state after electroweak symmetry breaking (EWSB). We focus on scalar Loryon models that acquire more than half the particle's mass from the Higgs mechanism and found four surviving BSM candidates using experimental bounds already established, including the scalar singlet and electroweak doublet, triplet, and quartet, all assumed to be colourless and carry additional $\mathbb{Z}_2$ charge to prohibit further decay. We recreate the tree-level HEFT mapping of a singlet scalar BSM under the above assumptions and show that it does not have a linearly realised Standard Model Effective Field Theory (SMEFT), which perturbs the vacuum before EWSB. We numerically calculated the cosmic relic density constraint with the current value of $\Omega_{DM}h^2 \sim 0.12$ on the mass m_s and Higgs portal coupling strength λ_s of the BSM scalar singlet and compared with the Loryon assumption, which rules out the resonant region around half Higgs-mass $m_s \sim m_h/2$. We compare the result with previous studies and conclude that only the high-mass $m_s \gg m_h/2$ islands survive for the BSM scalar singlet if we accept that dark matter receives most of its mass from the Higgs.

Except where specific reference is made to the work of others, this work is original and has not been already submitted either wholly or in part to satisfy any degree requirement at this or any other university. Link to the notebook.

Contents

Introduction

Dark matter (DM) was first predicted to explain the deviation between the observed galactic rotational curve and the Newtonian prediction in the 1930s [1–4]. However, we have not found the particles responsible for these effects.

The Effective Field Theory (EFT) framework can capture the properties of DM when studied as a beyond-the Standard Model (BSM) extension. An EFT comprises fields in the IR scale but expanded to higher order to encapsulate potential UV contribution. Fermi theory is a famous example that works to explain beta decay without needing $W^{\pm}$ boson as a mediator because the experiments did not reach Fermi theory's energy cutoff [5]. The same logic also works top-down; we can calculate the UV contribution to IR physics through the *matching* calculation, and constraining IR is the same as posing bounds on UV regardless of what model UV represents.

Using this idea, we can constrain BSM models that could describe DM using collider and astrophysical measurements. Our study focuses on the Standard Model Effective Field Theory (SMEFT) and Higgs Effective Field Theory (HEFT) frameworks, built using the same concrete blocks as the SM but to higher order expansion. The difference lies in the point of perturbation, where SMEFT expands from the vacuum before electroweak symmetry breaking (EWSB), while HEFT perturbs from the non-zero ground state.

At first glance, we might suspect HEFT can be expressed as SMEFT by field redefinition. However, in 1968, Coleman, Curtis, Wess, and Zumino (CCWZ) [6, 7] taught us that non-linearity is necessary for some theories after symmetry breaking, and this fact emerges when we try to understand the mapping between SMEFT and HEFT. The relation between the two has been extensively studied by Cohen, Craig, Lu, Sutherland (CCLS) [8], and its phenomenology with Banta [9]. Alonso, Jenkins, and Manohar also studied the geometric interpretation of the scalar sector Lagrangian and made the connection between non-analyticity and non-linearity that we find in HEFT [10, 11]. CCLS [12] used the interpretation to derive bounds on unitarity violation of HEFT.

Our study constitutes three parts. The first part focuses on the EFT construction, starting from section 1 discussing the separation of scales and basic EFT calculation we need before section 2 introduces the concept of non-linearity through the construction of a Lagrangian after symmetry breaking. Section 3 concludes the first part by presenting the definition and relation of SMEFT and HEFT. The second part starts with section 4 studying a BSM singlet scalar using tools we introduced and motivates the Loryon condition. Section 5 discusses UV Loryons allowed in DM physics. The final part includes section 6 summarising properties of thermal dark matter and how it contributes to UV constraints. Section 7 then concludes with the application of relic constraints on the singlet model, eliminating parts of the parameter space.

I Scale and EFT

1 Separation of scale

The idea of describing a physical system with only parameters local to its scale is not new, as Weinberg points out [13], this locality of either energy or length scale is implicit in all of Newtonian mechanics. The formal construction of the EFT involving renormalisation is beyond the scope of this work, and we will demonstrate the computation necessary for our current phenomenological study.

1.1 Scale separability

An EFT builds on the separability of scales of a theory's Lagrangian. We can see this in the SM, where from dimensional analysis we require $[S] = 0$ because the path integral partition function $\mathcal{Z} \sim \int d^4x \exp(iS)$ means the Lagrangian density has dimension $[\mathcal{L}] = 4$. Therefore, terms in the Lagrangian with a combination of fields that has a higher dimension than four must be suppressed by upper energy scale limit Λ, below which the theory is valid and renormalisable

$$\mathcal{L} \supset +\frac{g}{\Lambda^n}O^{(n+4)}, \tag{1.1}$$

where $[O^{(m)}] = m$, and we constructed g to be a dimensionless quantity and as pointed out before, Λ is the energy 'cut off' of the theory. A Lagrangian written this way is specified by the Wilson coefficients $\{c_i\}$ of $\mathcal{L} \supset c_i O^{(i)}$. The higher the energy cutoff means greater the higher order terms are suppressed, and in the case of the SM, the energy cutoff is magnitudes higher than the electroweak scale, which is why we are allowed to predict physics in the LHC by writing down only the first four order terms that preserve all the symmetries in SM. However, the higher order terms ($n > 0$) from a UV completion can still contribute to observations on the lower energy scale, and we can calculate its due correction by integrating the heavy particles from the UV theory. The magnitude of correction depends on the kinematic of the diagram we consider, and historic speculation of the effective field theory comes from the example of loop order correction. Appendix A describes an example of this in ϕ^6 theory.

1.2 Integrate heavy particles

We can take this a step further by considering an example of a general action S parameterised by both an IR- and UV-scale fields ϕ and Φ, with mass $m \ll M$ respectively, then the partition function of the path integral is

$$\mathcal{Z} = \int \mathcal{D}\phi \int \mathcal{D}\Phi \exp(iS_{\text{UV}}[\phi, \Phi]) = \int \mathcal{D}\phi \exp(iS_{\text{Eff}}[\phi]), \tag{1.2}$$

where we introduced the effective action, parameterised by only the lighter ϕ and independent of Φ that lives in the Λ scale. The heavier field Φ is said to be *integrated out* because the energy in the IR landscape cannot excite field Φ and does not contribute to additional scattering beyond multiplicative constant. The tree-level effective action S_{Eff}, derived in appendix A

$$S_{\text{Eff}}[\phi] = S_{\text{UV}}[\phi, \Phi_0], \quad \left.\frac{\partial V(\phi, \Phi)}{\partial \Phi}\right|_{\Phi_0} = 0, \tag{1.3}$$

which is the classical path of the heavy particle.

2 Non-linear realisation

The need for a non-linear Lagrangian that respects the broken symmetry and the unbroken global symmetry is more than just simplifying the algebra; it is necessary because some symmetry-broken fields can only be described by a non-linear theory, and affects the construction of its effective field theory as shown in AJM [10] and CCLS [8]. The goal is to find a theory using only the broken symmetry so we can carry out perturbation around the physical ground states.

The categorisation of non-linear gauge transformations [6] and consequently, the construction of the invariant Lagrangian [7] was worked out by CCWZ, which allow us to describe long-lived particles that gain most of their mass from the Higgs. We start by considering a global symmetry G that undergoes symmetry breaking to $H \subset G$ and introduce a set of basis $\{T^a\}$ that spans the Lie algebra $\mathfrak{h}$ of H and the broken generators $\{X^a\}$ spanning the rest of $\mathfrak{g}/\mathfrak{h}$. Together $\{T^a, X^b\}$ spans $\mathfrak{g}$. Since the residual symmetry $h \in H$ preserves the ground state $h\Phi_0(x) = \Phi_0(x)$ by definition, a general transformation $g(x) \in G$ acting on $\Phi_0(x)$

$$g(x)\Phi_0(x) = g(x)h\Phi_0(x), \tag{2.1}$$

is unique up to h. We can construct an equivalent class of $g(x) \sim g'(x)$ if there are $h \in \mathfrak{h}$ so that $g(x)h = g'(x)$, and CCWZ taught us that we can always build the theory's Lagrangian using only the set of broken generators

$$g(x) = e^{i\pi^a(x)X^a}, \tag{2.2}$$

and we should write our theory using $\{\pi^a(x)\}$ as the degrees of freedom. We know a similar fact from the Goldstone theorem, which says that under a broken symmetry G to H, we have $\dim G - \dim H$ massive particles and the massless Goldstone modes can be absorbed by gauge bosons. However, the CCWZ construction gives a concrete recipe for constructing the theory from knowledge of the symmetry alone.

Since $g(x)$ is local at each point if we perform a global transformation $\Omega \in G$ independent of x, it will likely map $g(x)$ to somewhere outside the coset, generally spanned by both $\{T^a, X^b\}$.

$$\Omega g(x) = g'(x), \quad g'(x) = e^{i\pi'^a(x)X^a} e^{iv^b(x)T^b}, \tag{2.3}$$

therefore, there always exists a local $h = e^{in^b(x)T^b}$ that can take us back to the coset we started from, depending on the transformation Ω,

$$g'(x) = \Omega g(x) h(x,\Omega)^{-1}. \tag{2.4}$$

Knowing how the symmetry action transforms in the broken basis, we can derive how different terms in the Lagrangian transforms under

$$\Phi(x) = g(x)\Phi_0(x) \rightarrow \Omega g(x) h(x,\Omega)^{-1}\Phi_0(x), \tag{2.5}$$

and so $|\Phi(x)|^2 \longrightarrow |\Phi(x)|^2$, which means the potential is preserved under global transformation, but the vector components concerning derivatives will have an extra term. Since any state $\Phi(x)$ can be specified by $\Phi(x) = g(x)\Phi_0(x)$, we can derive the transformation of a vector that is covariant around the origin before symmetry breaking

$$\begin{aligned} g^{-1}\partial_\mu g &\rightarrow h g^{-1}\Omega^{-1}\Omega(\partial_\mu g h^{-1} + g\partial_\mu h^{-1}) \\ &= h(g^{-1}\partial_\mu g)h^{-1} + h\partial_\mu h^{-1}. \end{aligned} \tag{2.6}$$

Because g lies in a local neighbourhood, $g^{-1}\partial_\mu g \in \mathfrak{g}$, we can decompose it in the basis of the remaining symmetry $\{T^a\} = \mathfrak{h}$ and the broken ones $\{X^a\} = \mathfrak{g}/\mathfrak{h}$,

$$g^{-1}\partial_\mu g = T^a \mathcal{V}(\pi)^a_\mu + X^b \mathcal{A}(\pi)^b_\mu, \tag{2.7}$$

substituting into equation (2.6), the two components transform separately. The transformation of $\mathcal{A}(\pi)_\mu = X^a\mathcal{A}(\pi)^a_\mu$ within the basis orthogonal of H

$$\mathcal{A}_\mu \rightarrow h\mathcal{A}_\mu h^{-1}, \tag{2.8a}$$

resembles the vector transformation, whereas the component in the residual symmetry $\mathcal{V}_\mu = X^b\mathcal{V}^b_\mu$ transforms as a covariant derivative

$$\mathcal{V}_\mu \rightarrow h\mathcal{V}_\mu h^{-1} + h\partial_\mu h^{-1}, \tag{2.8b}$$

which looks like a gauge field. What we have demonstrated is that the kinetic term in the unbroken phase $g^{-1}\partial_\mu g \in \mathfrak{g}$ transforms separately; the projection in $\mathfrak{h}$ is still the same covariant derivative, but the orthogonal part in $\mathfrak{g}/\mathfrak{h}$ becomes a covariant vector. We can therefore construct Lagrangian using the broken $\mathfrak{g}/\mathfrak{h}$ generators using $\mathcal{A}_\mu$, e.g. if $(\mathcal{A}_\mu)^2$ forms a singlet then we can trace over and write down our Lagrangian

$$\mathcal{L} \supset f^2\mathrm{Tr}(\mathcal{A}_\mu\mathcal{A}^\mu) + O(\mathcal{A}^4). \tag{2.9}$$

In the language of representation theory, $g^{-1}\partial g$ can be written in an irreducible form and split into subspace corresponding to $\mathfrak{h}$ and those orthogonal $\mathfrak{g}/\mathfrak{h}$. Since our field Φ transforms only under $\mathfrak{g}/\mathfrak{h}$ shown in equation (2.1) and (2.2), we are only concerned with the $\mathfrak{g}/\mathfrak{h}$ represented as $\mathcal{A}_\mu$, and we can build invariant elements by writing down copies of $(\mathcal{A}_\mu)^n$, same as we did in equation (2.9). We took a non-linear broken symmetry G/H due to the non-trivial $h(x,\Omega)$ function in equation (2.4), and broke it down into components that act linearly in H and absorb the non-linear part into gauge derivatives.

3 The geometry of a Lagrangian

Before the matching calculation, we need the Lagrangian with all terms respecting the symmetry of the fields. If the theory undergoes symmetry breaking, the Lagrangian perturbed around the non-zero ground state instead of the fixed point could be nonlinear. Since most particles gain their mass from the Higgs mechanism, the issue of non-linearity matters to the matching process.

3.1 SMEFT vs HEFT

Consider the Higgs field H under a global $SO(4) = (SU(2) \times SU(2))/\mathbb{Z}_2$ symmetry, which can be expressed as either

$$H = \begin{pmatrix} \phi_1(x) \\ \phi_2(x) \\ \phi_3(x) \\ \phi_4(x) \end{pmatrix}, \quad H = \begin{pmatrix} \phi_1(x) + i\phi_2(x) \\ \phi_3(x) + i\phi_4(x) \end{pmatrix}, \tag{3.1}$$

depending on the representation. In both cases we can construct the scalar components using linear combinations of $|H|^2$. Collect the terms by the number of derivatives

$$\mathcal{L}_{\text{SMEFT}} = \underbrace{-V(|H|^2) + A(|H|^2)\partial_\mu H^\dagger \partial^\mu H}_{\text{SM}} + B(|H|^2)\partial_\mu |H|^2 \partial^\mu |H|^2 + O(\partial^4), \tag{3.2}$$

which describes the SM Effective Field Theory (SMEFT) as the linear realisation of the Higgs interactions. SMEFT is linear because the perturbation around the origin restores electroweak symmetry and allows any order or operator that respects the field symmetry around the vacuum.[1] On the other hand, the Higgs Effective Field Theory (HEFT) is parameterised in the symmetry broken space as shown in figure 1. The parameterisation perturbs from the ground state

$$H \longrightarrow (v_0 + h(x))\hat{n}(x), \quad \partial_\mu H \longrightarrow \hat{n}\partial_\mu h + (v_0 + h)\partial_\mu \hat{n}, \tag{3.3}$$

where v_0 is the ground state energy and $\hat{n}$ is a unit radial vector in $S^3 \subset \mathbb{R}^4$, also denoting the gauge degree of freedom in the residual symmetry, while $h(x)$ is the physical field. We use the same notation as CCLS [8] and AJM [10] to write the HEFT expansion in kinetic terms of h and $\hat{n}$

$$\mathcal{L}_{\text{HEFT}} = \frac{1}{2}[K(h)]^2 \partial_\mu h \partial^\mu h + \frac{1}{2}[F(h)]^2 |\partial \hat{n}|^2 - V(h) + O(\partial^4). \tag{3.4}$$

In fact, we can show that any SMEFT can be written as a HEFT by substituting the parameterisation (3.3) to equation (3.2)

$$\begin{aligned} \mathcal{L}_{\text{SMEFT}} \longrightarrow &- V(h) + A(h)[\partial_\mu h \partial^\mu h + (v_0 + h)^2 \partial_\mu \hat{n} \partial^\mu \hat{n}] \\ &+ B(h)|\partial_\mu (v_0 + h)^2|^2 + O(\partial^4), \end{aligned} \tag{3.5}$$

[1] The same principle applies to other fields Φ under $U \in SU(N)$ if the perturbation is about the fixed point at the origin, the Lagrangian is a polynomial of $\Phi^\dagger \Phi \to \Phi^\dagger U^\dagger U \Phi = \Phi^\dagger \Phi$.

and the coefficient matching can be found as

$$\mathcal{L}_{\text{HEFT}} = [A(h) + 4B(h)(v+h)^2]|\partial h|^2 + A(h)(v_0+h)^2|\partial\hat{n}|^2 - V(h) + O(\partial^4); \tag{3.6}$$

however, the converse is not necessarily true. Although all SMEFT can be written as a HEFT, not all HEFT can be written as a SMEFT. The condition of whether the theory is exchangeable under field redefinition is studied in CCLS [8, 12] using both the unitarity condition and geometric properties of the scalar sector developed by AJM [10, 11], stating that a HEFT has a SMEFT expansion if the non-linear realisation has a new fixed point, around which the Taylor expansion is well-behaved. This fixed point corresponds to the vacuum origin that restores the electroweak symmetry.

Theorem 1 (AJM 2016, CCLS 2021)**.** *A HEFT has a SMEFT-like expansion if and only if*

1. *there exist $h_* \in \mathbb{R}$ so that $F(h_*) = 0$,*
2. *$K(h), F(h)$, and $V(h)$ all have convergent Taylor expansion around $h = h_*$,*
3. *the curvature $R(h_*)$ is finite,*

where R is the Ricci scalar of $\mathcal{L}_{HEFT}$ on the coordinate $(h, \hat{n})$,

where we can calculate the Ricci scalar by writing equation (3.6) as an invariant line element. Equipped with theorem 1, we can calculate whether a HEFT-representing theory has a convergent SMEFT-like expansion in the neighbourhood of a renewed fixed point h_*. However, having a well-behaved fixed point only guarantees the existence of linear realisation local to h_* up to some radius of convergence, which should cover the HEFT physical vacuum if the theory were to be truly SMEFT.

3.2 Convergence and unitarity

Following theorem 1, we can calculate the radius of convergence by looking for non-analytic poles of R, and the convergence radius is measured by how far the pole is from the point of expansion. The calculation relies on the geometric construction of the scalar sector by AJM [10, 11], where they use the scalar manifold $\mathcal{M}$ to describe a BSM extension. The SM itself describes a flat $\mathcal{M}$ with zero curvature, whereas BSM introduces deviation from the SM and non-zero curvature. Whether the BSM fields transform linearly or non-linearly under the unbroken/broken gauge group is irrelevant to the global structure of the theory and is a matter of field redefinition. However, the parameterisation has to preserve the global structure.

From a geometric standpoint, a HEFT will therefore contain a SMEFT-like structure if it has a new fixed point h_* corresponding to SMEFT's vacuum origin. Whether the expansion around the new fixed point covers the whole domain depends on the radius of convergence calculated using the sectional curvature $\mathcal{K}_i$, defined in appendix B, of the BSM manifold $\mathcal{M}$. The sectional curvature $\mathcal{K}(\Pi)$ is the Gaussian curvature of a plane Π in the tangent space $T_p\mathcal{M}$, independent of the choice of vectors in Π. The Ricci scalar is proportional to the sum of sectional curvature [12], and in simple cases such as the singlet

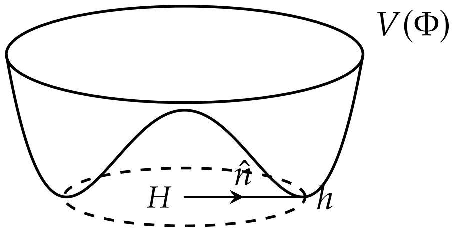

Figure 1: Parameterisation of the Higgs field before (H) and after (h, $\hat{n}$) symmetry breaking.

scalar, we can find the convergence radius by studying the Ricci scalar without consulting the analyticity of individual sectional curvature.

Additionally, CCLS [12] derived the scale of unitarity violation for HEFT, which relates to the radius of convergence of the sectional curvature $\mathcal{K}_h$, where h is the physical field as defined before. The proof is based on the Cauchy-Hadamard theorem that relates the radius of convergence of a function and its derivatives and found that the unitarity bound

$$E \lesssim 4\pi v_*, \tag{3.7}$$

for diagrams with two Higgs legs and v_* is the radius of convergence. As we will see in section 4.2, a scalar singlet has a valid SMEFT approximation if checked against theorem 1 up to the tree level. However, if the singlet acquires more than half its mass from EWSB, then it does not have a converging SMEFT and has to be described by HEFT.

II Dark Matter Candidates

4 The case of a scalar singlet

The singlet sector includes interaction with the Higgs, from which it acquires most of its mass through the symmetry breaking to the non-zero Higgs ground state, and if we allow the singlet to receive most of its mass from the Higgs, its EFT matches the non-linearly realised HEFT instead of SMEFT after EWSB. Without the gauge couplings, the Lagrangian of the singlet and Higgsis are as follows. We impose $\mathbb{Z}_2$ symmetry to avoid the additional Yukawa coupling with fermion doublets to ensure the singlet does not decay after freeze-out decoupling.

$$\begin{aligned}\mathcal{L}_{BSM} = &\partial_\mu H^\dagger \partial^\mu H + \mu_H^2 |H|^2 - \lambda_H |H|^4 \\ &+ \frac{1}{2}\partial_\mu S \partial^\mu S - \frac{1}{2} m^2 S^2 - \frac{1}{4}\lambda_S S^4 \\ &- \frac{1}{2}\lambda S^2 H^\dagger H,\end{aligned} \tag{4.1}$$

where the first two lines describe the free Higgs and singlet fields, and the last line is the singlet-Higgs coupling from which it receives mass after symmetry breaking. Both the Higgs and singlet live in a potential well with marginal terms, so to ensure the existence of the ground state, we require $\lambda_H, \lambda_S > 0$ and $\lambda^2 < 4\lambda_S\lambda_H$ because rewrite the fourth order terms

$$\left(\sqrt{\lambda_H}|H|^2 + \frac{\sqrt{\lambda_S}}{2}S^2\right)^2 + \left(\frac{\lambda}{2} - \sqrt{\lambda_S\lambda_H}\right)S^2|H|^2, \tag{4.2}$$

and we need the second term to remain positive. The singlet scalar field has a similar potential to the Higgs field, and symmetry breaking occurs if $m^2 < 0$ induces non-zero ground state energy v_s and creates the non-trivial tree level case satisfying

$$v_s(m^2 + \lambda_S v_s^2) = 0, \tag{4.3}$$

which we can perturb by setting $S \to v_s + s$ and $\partial_\mu S \to \partial_\mu s$. Substituting back to the Lagrangian and simplifying using the ground state condition (4.3), we can write down the following

$$\begin{aligned}\mathcal{L}_{BSM} = &\mathcal{L}_H + \frac{1}{2}\partial_\mu s \partial^\mu s \\ &- \frac{1}{2}(2v_s^2\lambda_s + \lambda|H|^2)s^2 - \frac{1}{4}\lambda_S s^4 \\ &- \frac{1}{2}v_s^2\lambda|H|^2 + 2v_s^3\lambda_s s + v_s\lambda|H|^2 s,\end{aligned} \tag{4.4}$$

where we collected the terms by power of the symmetry-breaking generator s. We can therefore identify the mass of the singlet scalar before the spontaneous symmetry breaking of Higgs in the second line, and again simplify using the vacuum expectation value $v_s^2 = -m^2/\lambda_S$ since $m^2 < 0$

$$m_s = \lambda|H|^2 - 2m^2. \tag{4.5}$$

4.1 Integrate heavy particle

We want to find the effective Lagrangian by integrating out the heavy singlet up to the tree level using equation (1.3) derived in appendix A, which means finding the classical solution to the potential $V(H,s)$ expanded around ground state

$$\left.\frac{\partial V(H,s)}{\partial s}\right|_{s_0} = 0 = \lambda_s s_0^3 + 3v_s\lambda_s s_0^2 + 2(\lambda_s v_s^2 + \lambda|H|^2/2)s_0 + v_s\lambda|H|^2, \tag{4.6}$$

which contains solutions

$$s_0 = -v_s, \quad s_0 = -v_s - \sqrt{v_s^2 - \frac{\lambda|H|^2}{\lambda_s}}, \quad s_0 = -v_s + \sqrt{v_s^2 - \frac{\lambda|H|^2}{\lambda_s}}. \tag{4.7}$$

The first solution represents the vacuum state, and the second solution is rejected because, without the Higgs field, the ground state should be equal to the vacuum state $s_0|_{H=0} = 0$. Substituting the third solution and $v_s^2 = -m^2/\lambda_s$ to the Lagrangian gives us the non-trivial EFT pre-EWSB

$$\mathcal{L}_{\text{Eff}} = \mathcal{L}_H + \frac{1}{2}\partial_\mu s_0 \partial^\mu s_0 - \frac{m^2\lambda}{2\lambda_s}|H|^2 + \frac{\lambda^2}{4\lambda_s}|H|^4 + \frac{m^4}{4\lambda_s}, \tag{4.8}$$

which we can expand and collect the Higgs term before expanding around the ground state

$$\begin{aligned}\mathcal{L}_{\text{Eff, pre-SB}} =& \partial_\mu H^\dagger \partial^\mu H + \mu_H^2|H|^2 - \lambda_H|H|^4 \\ &+ \frac{-\lambda^2}{8\lambda_s(m^2+\lambda|H|^2)}\partial_\mu|H|^2\partial^\mu|H|^2 + \frac{1}{4\lambda_s}(\lambda|H|^2+m^2)^2,\end{aligned} \tag{4.9}$$

independent of the BSM field s and only depends on the UV parameters, which presents a non-linear expansion around the Higgs vacuum state.

4.2 HEFT irreducibility

Using equation (3.6), the expansion around the Higgs ground state $H \to (h+v_0)\hat{n}/\sqrt{2}$

$$\begin{aligned}\mathcal{L}_{\text{HEFT}} =& \frac{1}{2}\overbrace{\left[1 - \frac{\lambda^2(v_0+h)^2}{2\lambda_s[2m^2+\lambda(v_0+h)^2]}\right]}^{K(h)^2}\partial_\mu h^\dagger \partial^\mu h + \frac{1}{2}\overbrace{(v_0+h)^2}^{F(h)^2}|\partial\hat{n}|^2 \\ &\underbrace{+\frac{1}{2}\mu_H^2(v_0+h)^2 - \frac{1}{4}\lambda_H(v_0+h)^4 + \frac{1}{4\lambda_s}\left[\frac{\lambda^2}{2}(v_0+h)^2+m^2\right]^2}_{V(h)} + O(\partial^4),\end{aligned} \tag{4.10}$$

and we can find out whether the non-linear description is necessary using theorem 1. Because $F(-v_s) = 0$ so $h_* = -v_s$ is a candidate for the fixed point. We can see that $K(h)$ has a convergent Taylor expansion by letting $\epsilon = v_0 + h$ and expand around $\epsilon \ll m\sqrt{\lambda}$, and the same applies for the potential $V(h)$. We can calculate the Ricci curvature on the coordinate system of $(h, \hat{n})$ by writing the derivative terms as a quadratic form. Specifically, since $\hat{n} = \left(n_1, n_2, n_3, \sqrt{1 - \mathbf{n}\cdot\mathbf{n}}\right)$, where $\mathbf{n} = (n_1, n_2, n_3)$,

$$\partial_\mu \hat{n} = \left(\partial_\mu n_1,\ \partial_\mu n_2,\ \partial_\mu n_3,\ \sum_{i=1}^{3} \frac{-n_i \partial_\mu n_i}{\sqrt{1-|\mathbf{n}|^2}}\right), \tag{4.11}$$

so the contracted term is

$$|\partial \hat{n}|^2 = \sum_{i=1}^{3} \partial_\mu n_i \partial^\mu n_i + \sum_{i=1}^{3}\sum_{j=1}^{3} \frac{n_i n_j \partial_\mu n_i \partial^\mu n_j}{1 - |\mathbf{n}|^2} = \left(\delta_{ij} + \frac{n_i n_j}{1 - |\mathbf{n}|^2}\right)\partial_\mu n_i \partial^\mu n_j, \tag{4.12}$$

and the metric is therefore separated in two subspaces between the h and $\hat{n}$, where the capital indices $I = \{h, 1, 2, 3\}$, and the lower case indices retain their original definition

$$g_{IJ} = \begin{pmatrix} K(h)^2 & 0 \\ 0 & F(h)^2\left(\delta_{ij} + \frac{n_i n_j}{1-|\mathbf{n}|^2}\right) \end{pmatrix}, \tag{4.13}$$

which split into the subspaces of one physical and three gauge dimensions, resonating with the CCWZ construction building the Lagrangian using broken symmetry in section 2. The perturbation from the SM introduces off-diagonal terms in the metric. We can therefore calculate the Ricci scalar using equation (A.9) in [8] and `Mathematica`

$$\begin{aligned} R &= -\frac{6}{K^2 F}\left[\partial_h^2 F - \partial_h F \frac{\partial_h K}{K}\right] + \frac{6}{v^2 F^2}\left[1 - \left(\frac{v}{K}\partial_h F\right)^2\right] \\ &= 6\lambda^2 \frac{\lambda(\lambda - 2\lambda_s)(h+v)^2 - 8m^2\lambda_s}{[\lambda(\lambda - 2\lambda_s)(h+v)^2 - 2m^2\lambda_s]^2}, \end{aligned} \tag{4.14}$$

At the fixed-point candidate, $h \to -v$, the Ricci scalar reduces to $R \to -12\lambda^2/m^2\lambda_s$, which only diverges if $m \to 0$, so a convergent SMEFT description around the neighbourhood of $h_* = -v$ exists on tree-level with non-vanishing m.

4.3 Convergence and Loryon

However, we need to ensure that the radius of convergence is at least around $\sim v$ to be expandable around the physical vacuum. We can calculate the radius by first finding where the curvature R diverges by setting the denominator of equation (4.14) to zero[2]

$$0 = \lambda(\lambda - 2\lambda_s)(h+v)^2 - 2m^2\lambda_s, \tag{4.15}$$

and so the diverging poles are at

$$h_p = -v \pm \sqrt{\frac{2m^2\lambda_s}{\lambda(\lambda - 2\lambda_s)}} = -v \pm i\sqrt{\frac{m^2}{\lambda(1 - \lambda/2\lambda_s)}}, \tag{4.16}$$

[2]The more mathematically rigorous approach involves decomposing the Ricci scalar into separate sectional curvatures described in appendix B and studying their convergence individually.

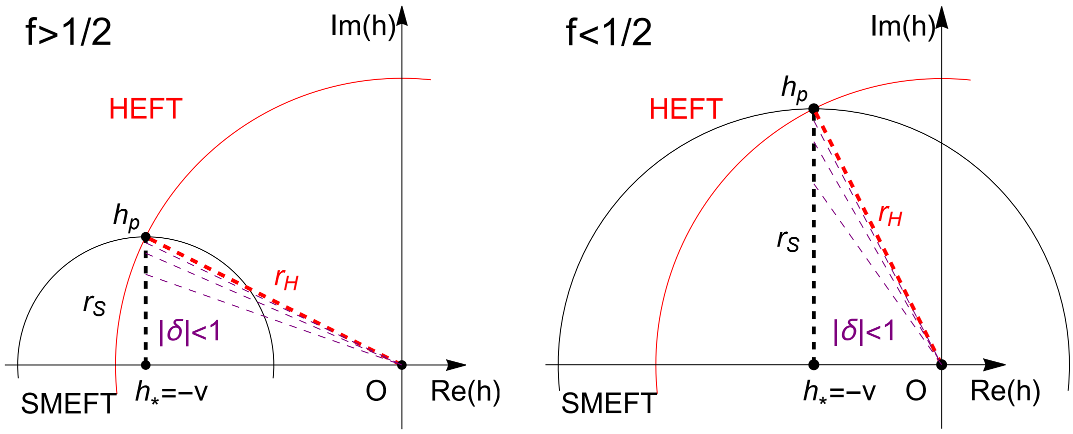

Figure 2: The two arcs demonstrate the radii of convergence for both SMEFT and HEFT in the two cases when the particles get most of their mass from the Higgs mechanism ($f > 1/2$) and otherwise ($f < 1/2$). The radii of convergence are measured from their respective origin of perturbation until the first non-analytic pole at $h_p = -v + \sqrt{2m^2/\lambda(1+\delta)}$. The purple dashed line shows the locus of $\delta = -\lambda/2\lambda_s$ as it approaches zero towards the physical solution. The SMEFT radius does not contain the origin if $f > 1/2$, so the theory is described by HEFT.

noting that since $\lambda\lambda_s < 0$, so $-\lambda/2\lambda_s > 0$. In practice, $-\lambda/2\lambda_s \to 0$ is a valid physical approximation [12] because the Higgs portal typically has stronger coupling than the BSM self-interaction. Therefore, we have two radii of convergence, and we choose the solution with a smaller modulus. The radii depending on the origin of the perturbation are

$$r_{\text{SMEFT}} = |h_p - h_*| \to \sqrt{\frac{2m^2}{\lambda}}, \quad r_{\text{HEFT}} = |h_p - 0| \to \sqrt{v^2 + \frac{2m^2}{\lambda}}, \tag{4.17}$$

where SMEFT is perturbed from the new fixed point h_*, and HEFT is from the origin. We introduce the ratio f of the percentage of EWSB contribution to the BSM mass

$$f = \frac{\lambda v^2/2}{m^2 + \lambda v^2/2}, \tag{4.18}$$

which means if $f > 1/2$, and the BSM singlet receives most of its mass from the Higgs. We can also rewrite $r_{\text{HEFT}} = v/\sqrt{f}$ and examine different regions of $f > 1/2$ and $f \leq 1/2$ as shown in figure 2. If $f > 1/2$, the radius of convergence centred at SMEFT ground state does not reach the origin, where HEFT perturbs from. Therefore the UV theory has to be described using HEFT and not SMEFT. Also, since AJM [11] showed the HEFT model has a cutoff due to unitarity violation of $W_L W_L \to W_L W_L$ and $W_L W_L \to hh$ scattering at the scale beyond $\Lambda \sim 4\pi v$, the unitarity cutoff is above the kinematic requirement to produce a physical BSM state with at least the energy of double the rest mass

$$E_{\text{kin}} = 2m_s = 2\sqrt{\frac{\lambda v^2}{2}\frac{1}{f}} \sim \sqrt{\lambda}v < 4\pi v, \tag{4.19}$$

where the last inequality was derived by [12] using similar unitarity constraint [11].

The study of a BSM scalar singlet showed us that if it acquires more than half its mass from EWSB, its EFT does not have a SMEFT expansion because the perturbation around the physical ground state lies outside the radius of convergence. The EFT is, therefore, necessarily non-linearly realised when we integrate out the heavy field. A similar condition applies more generally to other non-composite BSM fields proved in CCLS [8]. The class of particles receiving most of its mass from the Higgs are called *Loryons* and are described by HEFT. In the next section, we will describe the role of BSM Loryons in the context of DM physics.

5 Loryon as dark matter

Having understood the suitable EFT for a Loryon BSM field, we will investigate how this fits into the picture of dark matter (DM) phenomenology if we assume that DM is made of one field only, i.e., *non-composite*. The non-composite assumption means there is only one BSM field describing DM presented as a particle theory; however, there are likely other physical degrees of freedom within the dark sector such as the singlet-doublet [14], and deviation between non-composite predictions and experiments can be a gateway to understanding dark sector comopsition.

5.1 Dark sector extension

We assume DM is a single BSM field and gains most of its mass from EWSB because most SM particles do as well [9]. Therefore, our DM candidate is a HEFT and conforms to all the Loryon constraints already observed in the LHC. Hence, we assume it is bosonic because most fermionic fields are eliminated through a mixture of unitarity, electroweak precision, and Higgs coupling constraints [9]. Under these assumptions, we only have a handful of BSM candidates listed in table 1 showing each stage of selection using $(C, L)_Y$ to denote the SM charges of the BSM model; C and L are the SM charges for the colour $SU(3)_C$ and electroweak field $SU(2)_L$ separately and Y is the hypercharge on top of the third generator T^3_R.

In the DM context, we can also assume the BSM model is a colour singlet unless it propagates as a composite dark 'nucleon', violating the non-composite assumption, shown as the first arrow in table 1. We charge the BSM field with an additional $\mathbb{Z}_2$ symmetry so $\Phi_{\text{BSM}} \to -\Phi_{\text{BSM}}$, prohibiting Yukawa coupling with the other fermionic fields within the SM. These assumption guarantees a long decay lifetime and limits its decay channels. The relaxation of the $\mathbb{Z}_2$ condition is a subject of further study and will hopefully arise from future UV completion. Henceforth, the model is limited to self-coupling and Higgs portals, in addition to the kinetic gauge terms depending on its SM charges. The goal is to constrain individual surviving models.

If we also find bounds on the EFT, it would limit the UV generally. Banta, Cohen, Craig, Lu, Sutherland (BCCLS) [9] investigated this on BSM Loryons independent of the DM context, which we will outline including a brief theoretical review of the $h \to \gamma\gamma$ decay that illuminates properties of composite Loryons.

Bosonic

SM	$(1,1)_Y$	$(1,2)_Y$	$(1,3)_Y$	$(1,4)_Y$	$(1,L)_Y$	$(3,1)_Y$	$(3,2)_Y$
Fields	S_Y	Φ_{2Y}	Ξ_Y	Θ_{2Y}	$X_{L,Y}$	$\omega_{\lvert 3Y \rvert}$	Π_{6Y}

$\downarrow$

Colourless

SM	$(1,1)_Y$	$(1,2)_Y$	$(1,3)_Y$	$(1,4)_Y$	$(1,L)_Y$
Fields	S_Y	Φ_{2Y}	Ξ_Y	Θ_{2Y}	$X_{L,Y}$

$\cdots$

$\downarrow$

Collider Constraint

SM	$(1,1)_Y$	$(1,2)_Y$	$(1,3)_Y$	$(1,4)_Y$
Fields	S_Y	Φ_{2Y}	Ξ_Y	Θ_{2Y}

Table 1: The different charges carried by a BSM and their corresponding fields. The first arrow eliminates non-colour singlets in the DM context, and the second arrow eliminates through collider constraint and non-composition, resulting in only four candidates. The notation represents (Colour, Weak)$_Y$, so for example Φ_{2Y} is a colour singlet but a $SU(2)_L$ doublet.

5.2 Constraint scoreboard

Following the arguments in section 5.1, the BSM scalars charged under $\mathbb{Z}_2$ and appear in the Lagrangian as square modulus $|\Phi_{\text{BSM}}|^2$, so coupling with the Higgs field includes $\sim h|\Phi_{\text{BSM}}|^2$ after electroweak symmetry breaking and contributes scaling on the first loop level scattering

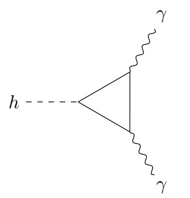

.

The same BSM effect also arises in Higgs-gluon decay $h \to gg$ but is irrelevant in DM modelling due to the colour singlet assumption. The first loop $h\gamma\gamma$ scaling is governed by the following Lagrangian post-EWSB

$$\mathcal{L} \supset -\frac{1}{2}\lambda_\Phi v h |\Phi_{\text{BSM}}|^2 = -f_\Phi \frac{m^2}{v} h |\Phi_{\text{BSM}}|^2, \tag{5.1}$$

where $f_\Phi = \lambda_\Phi v^2/2m^2$; here, m is the physical mass and f is the ratio of EWSB-mass defined before. The strength of the Φ_{BSM} field contribution and modifies the scaling of the $h\gamma\gamma$ vertex by κ_γ [9], noting that $\kappa_\gamma = 1$ in the SM

$$\kappa_\gamma \propto \sum_i f_i Q_i^2 A_{s_i}(\tau_i), \tag{5.2}$$

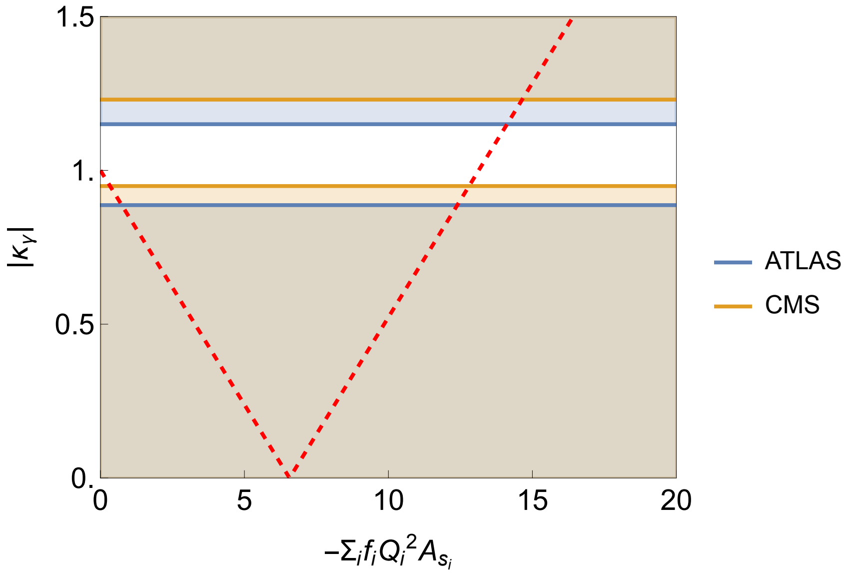

Figure 3: The ATLAS and CMS bounds on the scaling of the one-loop triangle Higgs photon decay $h\gamma\gamma$, where the red dashed line represents the value of $\kappa_\gamma \propto \sum_i f_i Q_i^2 A_{s_i}(\tau_i)$, which can still satisfy the $|\kappa_\gamma|$ condition if negative enough. However, this is only possible through a combination of fields using the spin $0, 1/2$ particles with negative form factors $A_{0,1/2}$ and is therefore impossible with only one BSM field. The SM charge product in the denominator of (5.6) is extrapolated from the BSM charge product bounds BCCLS [9] calculated. The experimental bounds can be improved in the projected precision measurement [15].

where i runs through all additional BSM fields, and Q is their electromagnetic charge. For our purpose $i = 1$ because there is only one Loryon field $\kappa_\gamma \propto f_\Phi Q^2 A_s(\tau)$, where s is the spin of the Loryon and $\tau = 4m_\Phi^2/m_h^2$ denotes the dimensionless mass. The experiments measure the deviation using form factors A_s given by, [9]

$$A_0(\tau) = \tau[1 - \tau F(\tau)], \tag{5.3a}$$

$$A_{1/2}(\tau) = -2\tau[1 + (1 - \tau)F(\tau)], \tag{5.3b}$$

$$A_1(\tau) = 2 + 3\tau[1 + (2 - \tau)F(\tau)], \tag{5.3c}$$

for different spins, where

$$F(\tau) = \begin{cases} \arcsin^2\left(1/\sqrt{\tau}\right), & \tau \geq 1 \\ -\frac{1}{4}\left[\log\frac{1+\sqrt{1-\tau}}{1-\sqrt{1-\tau}}\right]^2, & \tau < 1 \end{cases} . \tag{5.4}$$

We are only concerned with the scalar fields of spin 0 and 1, and from the discussion in section 5.1, the heavy BSM particles all have $\tau > 1$ because they acquire more than half their mass from the Higgs vev and $\tau \to \infty$ is a good approximation as numerically

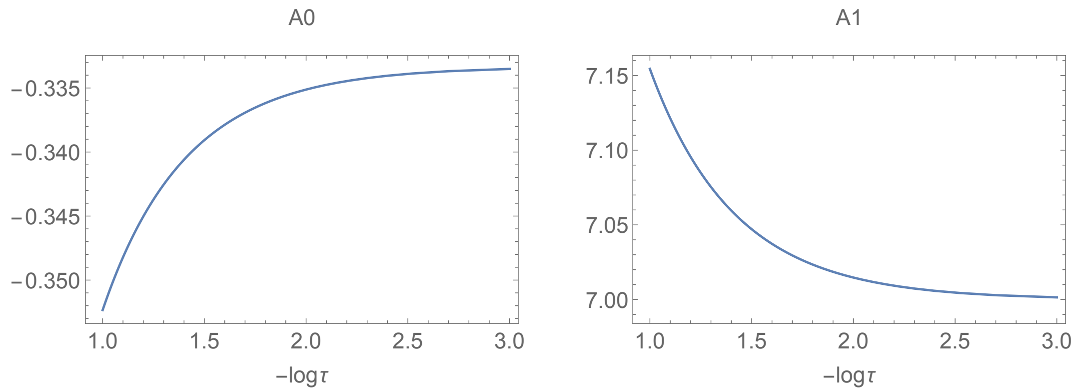

Figure 4: The plot is calculated using Taylor expansion around $A_{0/1}(\tau_0)$ at each point to demonstrate convergence as $\tau \to \infty$, showing $A_0 = -1/3, A_1 = 7$ within $\sim 1/10$ agreement.

demonstrated in figure 4

$$A_0 \to -\frac{1}{3}, \quad A_1 \to 7, \quad \tau \to \infty. \tag{5.5}$$

The vertex rescaling κ_γ can therefore be calculated by weighting the BSM contribution against the SM

$$\kappa_\gamma = 1 + \frac{f_\Phi Q^2 A_s(\tau)}{\sum_{\text{SM}} f_i Q_i^2 A_{s_i}(\tau_i)}. \tag{5.6}$$

The measurement from CMS [16] and ATLAS [17] bound the values allowed for $|\kappa_\gamma|$, and from face value, the CMS and ATLAS constraints require the charge product to be small so that $|\kappa_\gamma|$ stays close to unity. However, the sum of a composition of Loryon fields can satisfy the bounds on $|\kappa_\gamma|$ if some of its form factors are negative, as shown in figure 3. A number of Loryon fields, therefore, have more allowed SM charges, which is not allowed if we only introduce one BSM field. We extend this discussion on BSM fields to the custodial symmetry post-EWSB $SU(2)_{L/R}$ and introduce $[L, R]_Y$ denoting the representation in each residual field. Table 2 deduced from [9] shows the allowed SM charges of Loryons after Higgs coupling, which we updated to only allow non-composite models. The "$\sim$" denotes allowed hypercharge if the BSM model has access to Loryon composition, whereas "$\times$" completely rules out the possibility.

In summary, assuming non-composite DM acquiring at least half its mass from the Higgs with no colour charge results in unitarity, electroweak, and Higgs loop bounds forbidding most custodial charges apart from the eleven representations in table 2, which in SM charges can be calculated using the formula [9]

$$[L, R]_Y = \{(C, L)_{-\frac{R-1}{2+Y}}, \ldots, (C, L)_{\frac{R-1}{2+Y}}\}, \tag{5.7}$$

in steps of unit hypercharge. Regardless of hypercharge, we have four remaining candidates: scalar singlet and electroweak doublet, triplet, and quartet, as shown in the last

Scalar Scoreboard

	$R=1$	2	3	4	5	6	7	8
$L=1$	$\|Y\|=1$	1/2	0	$\sim$	$\sim$	$\sim$	$\sim$	$\times$
2	1/2	1	1/2	0	$\sim$	$\sim$	$\sim$	$\sim$
3	0	1/2	0	$\sim$	$\sim$	$\sim$	$\sim$	$\times$
4	$\sim$	0	$\sim$	$\sim$	$\sim$	$\sim$	$\times$	$\times$
5	$\sim$	$\sim$	$\sim$	$\sim$	$\sim$	$\times$	$\times$	$\times$
6	$\sim$	$\sim$	$\sim$	$\sim$	$\times$	$\times$	$\times$	$\times$
7	$\sim$	$\sim$	$\sim$	$\times$	$\times$	$\times$	$\times$	$\times$
8	$\sim$	$\sim$	$\times$	$\times$	$\times$	$\times$	$\times$	$\times$

Table 2: The representation of non-composite scalar Loryon that satisfies the Higgs one-loop decay $h\gamma\gamma$ and other unitarity and electroweak precision constraints. The fields with a "$\times$" means eliminated, and a "$\sim$" means there are allowed composite Loryons forbidden in our model. This table is derived from the complete scoreboard in Table 9 of BCCLS [9].

arrow of table 1. The electroweak doublet is especially well-studied as a DM model [18–21]. We will further constrain the UV models using the thermal properties of DM in the next section.

III Cosmic Relic

6 Thermal dark matter

Two general processes govern the balance of DM particles in the early universe. If the DM content is dense enough in the early universe, they can collide with each other and produce SM particles depending on their interaction Lagrangian. We call this process *inelastic* scattering as opposed to the *elastic* scattering as shown in figure 5, where a DM particle scatter off an SM particle and the density remains unchanged. The Boltzmann equation governs the balance of the two scattering processes [22], equating the covariant change due to universal expansion and the rate of annihilation.

We can repackage the two sides of the equation so that the density change only depends on the scattering cross section, containing all the BSM physics

$$\dot{n}_\chi + 3Hn_\chi = \langle \sigma v_{\chi\bar{\chi}} \rangle (n_{eq}^2 - n_\chi^2), \tag{6.1}$$

where n is the number density and H is Hubble's constant. n_{eq} is the density solution if the particles are in thermal equilibrium with the universe, and as promised, $\langle \sigma v_{\chi\bar{\chi}} \rangle$ is the thermal average cross-section containing DM interaction with the SM. The derivation following [23] is outlined in appendix C. Some key assumptions we made include time reversal invariance (equivalently CP) of the scattering process to ensure $|M_{\chi\bar{\chi}\to X\bar{X}}|^2 = |M_{X\bar{X}\to\chi\bar{\chi}}|^2$ and that the SM products are in thermal equilibrium with the universe at all times. Regarding the energy scale, we assume $T_i \ll E_i - \mu_i$ so the kinetic energy triumphs over chemical potential so Bose condensation/Dirac degeneracy does not happen.

We also introduce normalised number density $Y = n/s$, which is number density n divided by the entropy density s. The overall entropy is constant, so s tells us how much the universe has expanded. Also, the universe cools as it expands and the length scale a decides the temperature $T \propto 1/a$, which measures time, and we use rescaled time $x = m/T$ as the independent variable scaled by a characteristic mass, chosen as DM mass. Using $H = \dot{a}/a$ we can derive

$$\frac{dY}{dx} = \frac{s\langle \sigma v \rangle}{xH}(Y_{eq}^2 - Y^2), \tag{6.2}$$

which includes asymptotic regions that formalise the *freeze-out time* x_f at which inelastic scattering ceases, which can be approximated by

$$x_f \approx \ln[0.038(g_* x_f)^{-1/2} M_{PL} m_s \langle \sigma v \rangle], \tag{6.3}$$

where g_* is the particle degrees of freedom and M_{PL} is the Planck mass. If the freeze out x_f happens late enough that DM becomes non-relativistic or *cold*, its density in equilibrium

(a) Elastic scattering (b) Inelastic scattering

Figure 5: DM χ scattering through Higgs channel into SM particles X

leads to the leftover density we have today, called *cosmic relic density*. Appendix C derives its relation with the cross-section and freeze-out time

$$\Omega h^2 = \frac{1.07 \times 10^9 x_f}{g_*^{1/2} M_{PL} \langle \sigma v \rangle}. \tag{6.4}$$

Figure 6 demonstrates the departure of normalised density after decoupling time x_f for DM species of different cross sections, decided by the BSM coupling between DM and SM. We can also solve for the freeze-out time and cross-section at a fixed mass using equation (6.3) and (6.4) alone with a measurement of the relic density, as demonstrated in figure 7. The final piece of the jigsaw is calculating the thermal cross section using UV parameters. The calculation depends on the thermal properties of the incoming particles, which we assume are individually a canonical ensemble of the universal reservoir. Therefore, we can use the thermal integral developed by Gondolo and Gelmini [24, 25], outlined in appendix C

$$\langle \sigma v \rangle = \frac{x}{16 m_s^5 K_2^2(x)} \int_{4m^2}^{\infty} \sigma v \cdot s \sqrt{s - 4m^2} K_1(\sqrt{s}/T) ds, \tag{6.5}$$

where K_i are Bessel functions of second order and the integral is evaluated numerically.

7 The singlet relic

Observational DM exists independent of the UV theory, and we can formulate these constraints independent of the physics governing DM, including the thermal formulation of DM relic density measured by Planck Collaboration [26]. We will now consider the case of a scalar singlet as a thermal DM as we did in section 4 demonstrating the necessary non-linearity of the EFT if the BSM extension obtains most of its mass from electroweak symmetry breaking. We also showed that there are a limited number of surviving BSM models after elimination by collider constraints in section 5, which we can enumerate and apply thermal bounds on its UV parameter space. We reiterate the BSM Lagrangian that includes a $\mathbb{Z}_2$ symmetry to avoid Yukawa coupling

$$\mathcal{L}_{DM} = \frac{1}{2}\partial_\mu S \partial^\mu S - \frac{m^2}{2} S^2 - \frac{\lambda}{2} S^2 \mathrm{Tr}(H^\dagger H) - \frac{\lambda_s}{4} S^4, \tag{7.1}$$

where the BSM carries no SM charges and couples to the SM only through the Higgs portal; m and λ constitute the UV parameter space apart from the self-interaction λ_s,

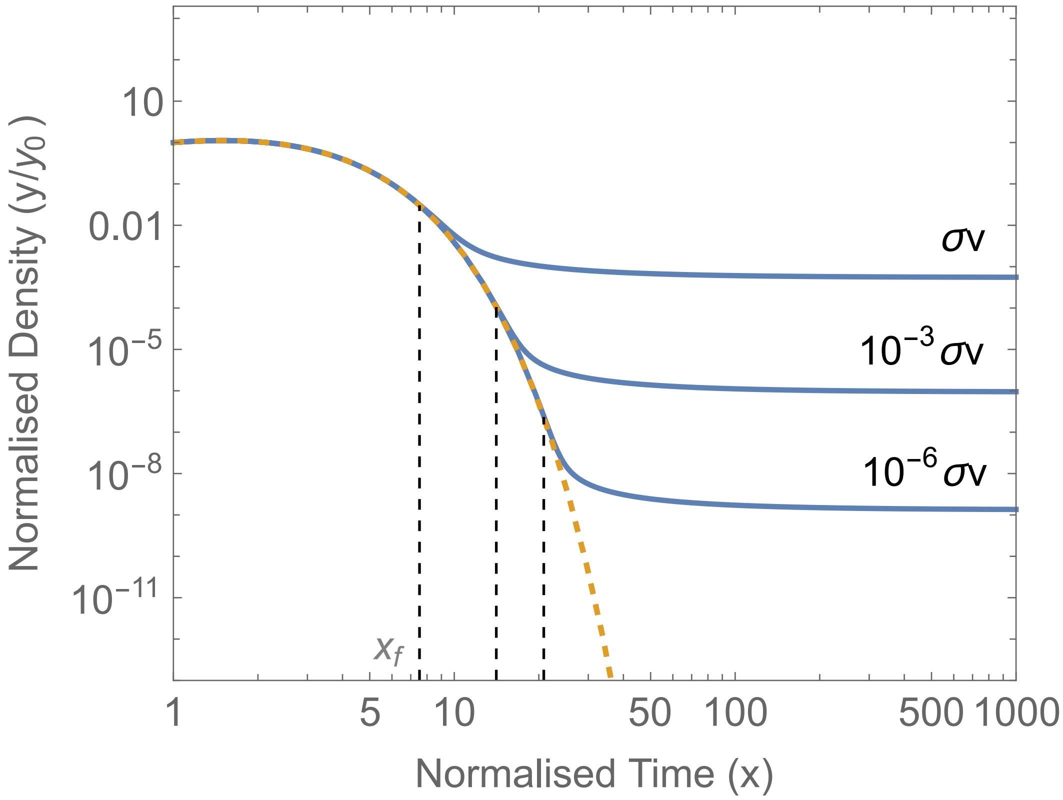

Figure 6: The evolution of relic density for three cross-sections is shown on normalised axes. The dashed curve represents the equilibrium solution, and the solid lines are the numerical solutions. The actual density departs from the equilibrium at freeze-out time x_f calculated using (6.3). The three solutions correspond to three particles with the same mass but different cross-sections, or coupling to SM equivalently.

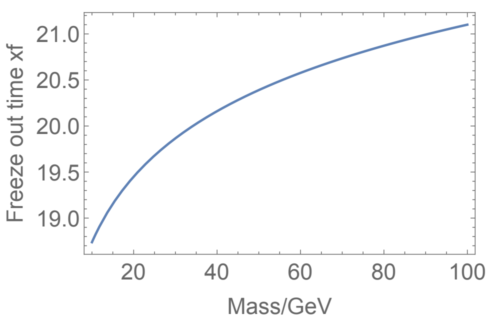

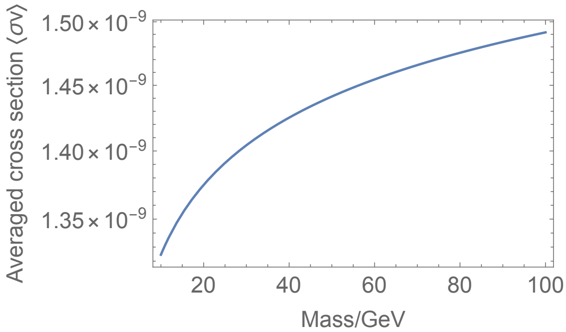

Figure 7: The freeze out time and averaged cross section for a particular mass can be solved analytically using equation (6.4) and (6.3) at a fixed mass with measurement of Ωh^2, which we took as 0.12 from Planck Collaboration [26]. The solutions are shown from below the resonant mass scale $m_s = m_h/2$ to above.

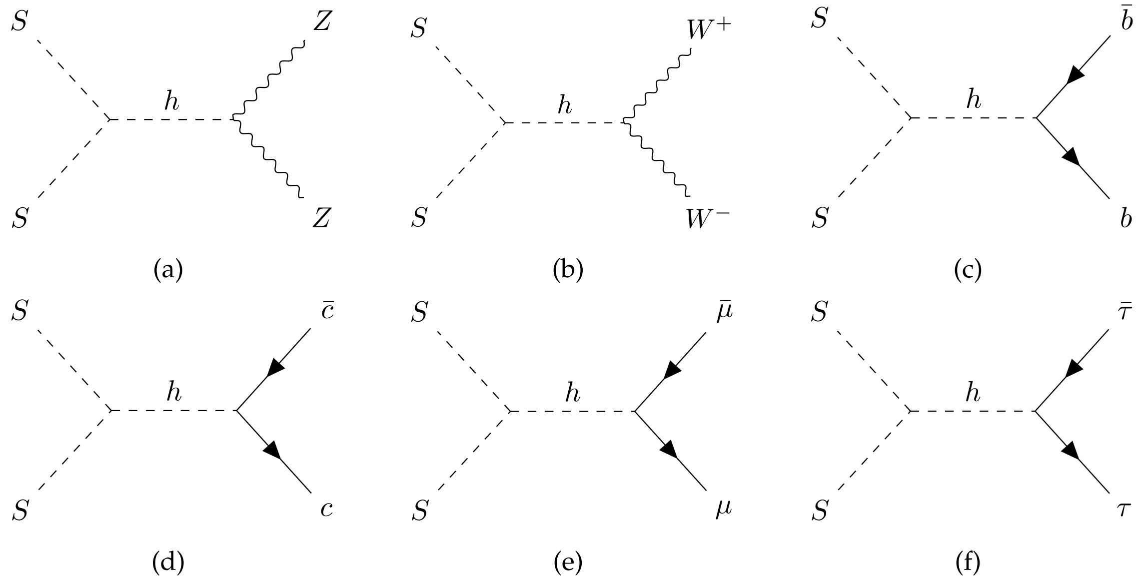

Figure 8: Higgs portal annihilation between two DM candidate in the singlet-scalar BSM extension. The allowed decay species are calculated using FeynArts, including lepton and quark decays. The $h \to e^- e^+, u\bar{u}, d\bar{d}$ channels are omitted here because the tree-level vertices are proportional to mass, so their branching ratio is suppressed by their lighter mass, e.g., $m_e/m_Z \sim 10^{-5}$.

which in electroweak scattering would be dominated by the Higgs portal. We saw in section 4 that the self-interaction term allows the possibility of non-trivial perturbation around the fixed point if we expand around the Higgs ground state instead of the vacuum state, so if we consider the Ricci scalar without self-interaction

$$R = 6\lambda^2 \frac{\lambda(\lambda - 2\lambda_s)(h+v)^2 - 8m^2\lambda_s}{[\lambda(\lambda - 2\lambda_s)(h+v)^2 - 2m^2\lambda_s]^2} \to 6, \tag{7.2}$$

which introduces finite, positive curvature and is analytic everywhere, so it has a linear representation as we might expect. Note that SM has Ricci scalar of 0 and the finite curvature measures our theory's deviation from SM. The post-EWSB Lagrangian also includes terms such as $\mathcal{L} \supset \lambda s^2 h^2/2$, which allows direct interaction producing two physical Higgs. Direct contact has a subdominant contribution to the inelastic process because further decay to the SM signal introduces additional suppressing vertex. However, the direct contact is enhanced if $m_h \gg m_s$, meaning the BSM singlet lies in the light-mass region eliminated by GAMBIT collaboration [27]. The dominant process for heavy singlet is, therefore, $ss \to h \to XX$, and the matrix element corresponding to the annihilation vertex is

$$|M|^2 \propto \frac{\lambda^2 v^2}{[(p_1+p_2)^2 - m_h^2]^2} = \frac{\lambda^2 v^2}{[s^2 - m_h^2]^2}, \tag{7.3}$$

while the most calculation-efficient way to include the second vertex is by introducing a transient term contributed by each Higgs portal, shown in figure 8 and derived using

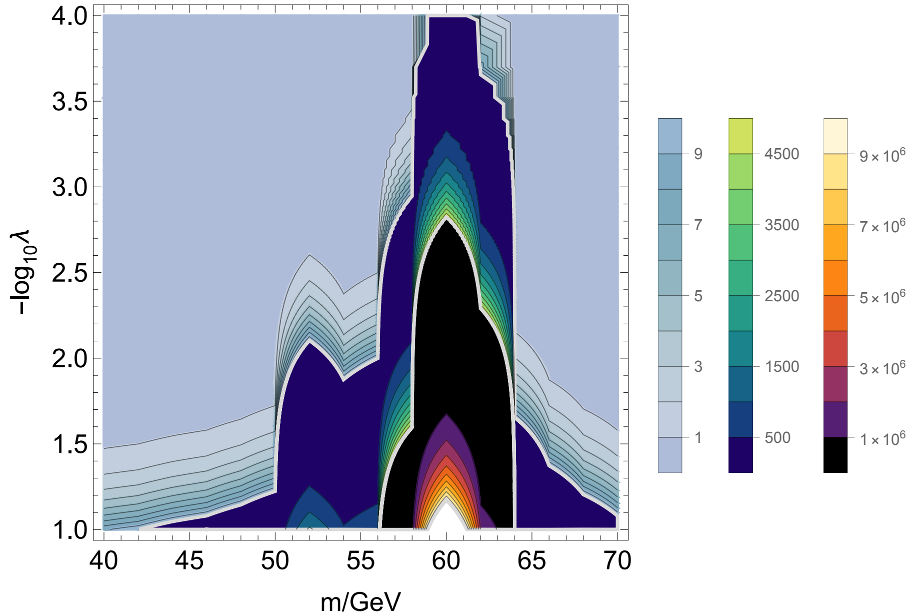

Figure 9: The contour of the thermal average of the cross-section in units of 10^{-9} across the singlet parameter space, constituted by the BSM mass m and coupling strength λ only. We can see the dependence between the two variables along each given cross-section, which we can use to fix the coupling strength of a given mass range. The differently shaded contours represent regions with a difference in magnitudes. Our theory is likely to lie within the out-most edge in blue tone, while it quickly diverges as we approach the resonant peak at the centre.

Breit-Wigner distribution [28]. The dominating interaction cross-section is

$$\sigma v = \frac{2\lambda^2 v^2}{[s^2 - m_h^2]^2 + m_h^2\Gamma_h^2}\frac{\Gamma_{hXX}}{\sqrt{s}}, \quad \sigma v_{\text{total}} = \frac{2\lambda^2 v^2}{\sqrt{s}\left[(s - m_h^2)^2 + m_h^2\Gamma_h^2\right]}, \tag{7.4}$$

where Γ_{hXX} is the branching ratio of a Higgs decaying into species X, e.g., Γ_{hbb} is the branching ratio of $h \longrightarrow b\bar{b}$. We can therefore substitute $\langle\sigma v\rangle_{\text{total}}$ into thermal integral developed by Goldolo and Gelmini [24] in equation (6.5) and calculate corresponding constraints on m_s and λ_s. Figure 9 shows the contours of thermally averaged cross-sections in the parameter space, which can be further constrained by measurements such as the relic abundance [26] or the XENON nucleon recoil measurement [29].

7.1 Singlet scalar constraint

We can obtain the relic constraint using (6.5) as shown in figure 10, which agrees with the trend of calculation first carried out in Burgess [30] with updated Higgs mass and coupling measurements [16, 17, 31]. We see a distinct peak around the half Higgs mass $m_s = m_h/2$ area as we would expect. Additionally, the Loryon model requires BSM

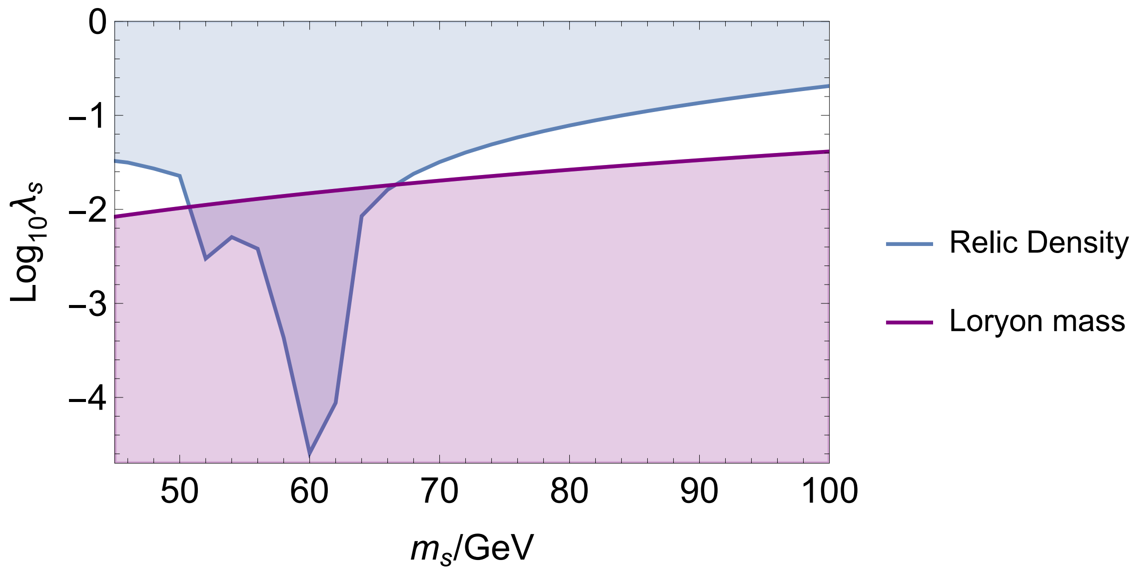

Figure 10: Constraining the scalar singlet model using both cosmic relic density measured by the Planck Collaboration [26] and Loryon mass. If we allow composite DM, the singlet can have weaker Higgs portal coupling yet maintain the same cross-section. The Loryon condition in this study requires the BSM particle to gain more than half its mass from the Higgs symmetry breaking, imposing a condition $\lambda > m_s^2/v^2$ on the allowed coupling strength. The unitarity bound on HEFT is $\lesssim 4\pi v \sim 3$TeV, which is way above the resonant region. The bounds eliminate much of the parameter space, leaving only the low-mass region eliminated by GAMBIT [32] and high-mass islands that could be probed by XENON [29].

extensions to acquire more than half their mass from the electroweak symmetry breaking

$$f = \frac{\lambda v^2/2}{m_s^2} > \frac{1}{2} \Rightarrow \lambda > \frac{m_s^2}{v^2}, \tag{7.5}$$

which is illustrated in figure 10 together with the relic constraint. The outcome contains two surviving regions in the parameter space.

The GAMBIT collaboration [27, 32–35] surveyed the scalar singlet model independent of the Loryon assumption while equipped with a $\mathbb{Z}_2$ protection from further decay across the same parameter space as we just described; the analysis found two surviving regions including the Higgs resonance eliminated by the Loryon constraint; and a high mass island in the parameter space still to be investigated [36]. However, the region is also bounded by HEFT unitarity $\lesssim 4\pi v \sim 3$TeV. One of the most prominent direct detection experiments for DM is XENON [29], which will hopefully survey the high mass regions [37] in the future and unveil its nature.

Conclusion and Outlook

We investigate the possibility of describing the dark matter as a BSM extension made of only one field of unknown SM charges. We assume that dark matter gains most of its mass from the Higgs mechanism, as do most SM particles, and describe it using HEFT after demonstrating that its EFT description is necessarily non-linear. We compared the DM model against the phenomenological study by BCCLS [9] and found that under the non-composite and colourless assumption, only four $(1,1), (1,2), (1,3), (1,4)$ SM charges survive after collider constraints, including one-loop κ_γ coupling from CMS [16] and ATLAS [31]. We also employed an additional $\mathbb{Z}_2$ symmetry to protect DM from fermionic Yukawa decay and maintain its long lifetime.

The relic density observation provides an upper bound on the UV parameters of DM if we assume it is non-composite. We numerically calculated the relic constraints using updated data from Planck [26], ATLAS [17, 31], and CMS [16]. We focus on the BSM extension of a scalar singlet which has to be described by HEFT instead of SMEFT using the geometric interpretation of kinetic scalar Lagrangian as prescribed in [12]. We showed that as one of the four surviving UV models, there are regions of parameter space that survive under relic constraint and the Loryon mass condition. The near resonance region is forbidden if the BSM singlet is a Loryon, which leaves the low mass eliminated by GAMBIT [27, 32–35] and the high mass partly surviving below the unitarity violating scale of ~ 3TeV [12].

A future study would include constraining the other three surviving Loryons using the relic method established and incorporating new HEFT techniques [38]. New measurements are projected to probe surviving regions [27, 32] and could one day answer:
"Does dark matter receive most of its mass from the Higgs?".

Acknowledgement

The candidate would like to thank Dr T You for hosting and guiding the ideas of this research project and Dr J Talbert for his supervision and continuous support throughout the research process. The candidate would also like to thank their colleagues at Cambridge Pheno Working Group and CERN-TH for their support and inspiration.

A Regulator and heavy particle

A.1 Dimensional regulator

Consider a first-loop order correction to the ϕ^4 theory including a ϕ^6 term

$$\mathcal{L} = \mathcal{L}_{\phi^4} + \frac{1}{6!}\frac{g_6}{\Lambda^2}\phi^6, \tag{A.1}$$

which means the first-loop order correction get integrated up to the UV cutoff, which contributes additional Λ in the numerator and means the correction is no longer suppressed

$$\delta i\mathcal{M} = \frac{1}{6!}\frac{g_6}{\Lambda^2}\int^{\Lambda}\frac{d^4k}{\mathcal{N}}\frac{1}{k^2-m^2} \sim \frac{g_6}{\Lambda^2}\frac{\Lambda^2}{\mathcal{N}}. \tag{A.2}$$

We get around this issue by instead integrate up to $\Lambda/m \to \infty$ and introduce a *dimensional regulator* ϵ, such that $d = 4-\epsilon$. We can therefore use the generalised thin-shell equation to ward off the divergence

$$\delta i\mathcal{M} = \int_0^{\infty}\frac{dkd\Omega}{\mathcal{N}'}\frac{k^{d-1}}{k^2-m^2} \sim \int_0^{\infty}\frac{dkk^{3-\epsilon}}{k^2-m^2} = \frac{-m^2\pi}{2m^{-\epsilon}\sin(\pi\epsilon/2)}. \tag{A.3}$$

Although the integral diverges with vanishing $\epsilon \to 0$, a finite-valued dimensional regulator $\epsilon > 0$ protects us from divergence and let us carry out loop-level correction from higher dimensional terms that are suppressed by the theory's energy scale.

A.2 Integrate-out heavy particles

The partition function of the path integral is

$$\mathcal{Z} = \int\mathcal{D}\phi\int\mathcal{D}\Phi\exp(iS_{\mathrm{UV}}[\phi,\Phi]) = \int\mathcal{D}\phi\exp(iS_{\mathrm{Eff}}[\phi]). \tag{A.4}$$

The heavier Φ field can only exist as an off-shell virtual particle through the propagator, which we can calculate by finding the effective action S_{Eff}, which we would like to match up to certain derivative order

$$S_{\mathrm{Eff}}[\phi] = S_{\mathrm{UV}}[\phi,\Phi_0] + \frac{\delta S_{\mathrm{UV}}[\phi,\Phi]}{\delta\Phi}\bigg|_{\Phi_0}\delta\Phi + \mathcal{O}(\delta\Phi^2), \tag{A.5}$$

which means that up to the first order $S_{\mathrm{Eff}}[\phi] = S_{\mathrm{UV}}[\phi,\Phi_0]$ given the second term vanishes, satisfying the classical equation of motion for the heavier field Φ that we can expand in powers of the derivatives involved in the Lagrangian using the same notation as [8]

$$\frac{\delta S_{\mathrm{UV}}[\phi,\Phi]}{\delta\Phi}\bigg|_{\Phi_0} = 0, \quad S_{\mathrm{UV}}[\phi,\Phi] = \sum_{m=0}^{\infty}S_{\mathrm{UV}}^{(2m)}[\phi,\Phi], \tag{A.6}$$

where $S_{UV}^{(0)} = \int -V(\phi,\Phi)d^4x$ is the Lagrangian potential without derivatives. This means that to match the tree-level UV-completion correction to the effective field, we have only

$$S_{\mathrm{Eff}}[\phi] = S_{\mathrm{UV}}[\phi,\Phi_0], \quad \frac{\partial V(\phi,\Phi)}{\partial\Phi}\bigg|_{\Phi_0} = 0, \tag{A.7}$$

which we can also use to calculate the Wilson coefficient if there are any non-zero non-renormalisable terms.

B Sectional curvature

We first consider the covariant derivative in a space with metric ${g^a}_b$ that lives in manifold $\mathcal{M}$

$$\nabla_a v_b = \partial_a v_b - {\Gamma^d}_{ba} v_d, \tag{B.1}$$

so we can derive the Rieman tensor ${R^d}_{abc}$ by anti-commuting the double derivative $\nabla_c \nabla_b v_a - \nabla_b \nabla_c v_a = {R^d}_{abc} v_d$ and factor out the dummy variable v

$${R^d}_{abc} = \partial_b {\Gamma^d}_{ac} - \partial_c {\Gamma^d}_{ab} + {\Gamma^e}_{ac} {\Gamma^d}_{eb} - {\Gamma^e}_{ab} {\Gamma^d}_{ec}, \tag{B.2}$$

We can calculate the Ricci tensor by contracting the first and last indices ${R^d}_{abd} = R_{ab} = R(a, b)$, where we changed the notation to emphasise that R is described in basis $a, b \in T_p\mathcal{M}$. Then for tangent space at $p \in \mathcal{M}$, spanned by basis $x, y = T_p\mathcal{M}$ we can define sectional curvature

$$K(x, y) = \frac{g(R(x, y)x, y)}{g(x, x)g(y, y) - g(x, y)^2}, \tag{B.3}$$

which is unique for each plane regardless of the choice of basis and is equivalent to the Gaussian curvature of surface Π. Therefore, the sectional curvature is sometimes written as $K(\Pi)$, where $\Pi \in T_p\mathcal{M}$ is a plane in the tangent space. Note that if x, y are orthonormal $g(x, y) = 0$ and $g(x, x) = g(y, y) = 1$ then

$$K(x, y) = g(R(x, y)x, y). \tag{B.4}$$

The sectional curvature essentially measures the change of a basis "plane" transported along a geodesic, and since the Ricci curvature describes the change of the "volume", it is the sum of the sectional curvature if we consider first order change. If we choose one direction x, then its orthogonal space is spanned by $n - 1$ orthonormal basis $\{e_i\} = \mathcal{B}$, where $\mathcal{B} \cup \{x\}$ spans $T_p\mathcal{M}$

$$\begin{aligned} R(x, y) =& g(R(x, x)x, x) + \sum_{e_i \in \mathcal{B}} g(R(x, e_i)x, e_i) \\ =& 0 + \sum_{e_i \in \mathcal{B}} K(x, e_i) = \sum_{e_i \in \mathcal{B}} K(x, e_i). \end{aligned} \tag{B.5}$$

Hence, the sum of sectional curvatures is proportional to the Ricci curvature. Some definitions include a $1/(n - 1)$ and define the Ricci curvature as the average of the sectional curvatures. The Ricci scalar can therefore be calculated using the trace of the Ricci curvature.

C Thermal equations

C.1 The Boltzmann equation

We can write down the equation governing the change of number density using the Boltzmann equation [22, 23], which equates to the covariant change due to the universe expansion

$$L[f] = C[f], \tag{C.1}$$

where L is the Louville operator governing the covariant change and C is the collisional contribution. As the universe expands, the density of DM dilutes and its covariant change

$$L[f] = E\frac{\partial f}{\partial t} - \frac{\dot{a}}{a}|\mathbf{p}|^2\frac{\partial f}{\partial E}, \tag{C.2}$$

where f is the density in phase space $f = f(\mathbf{v}, \mathbf{x})$, and a is the expansion rate in the Friedman-Walker metric, assuming that space is isotropic at each time slice. By definition, the phase space density f relates to the number density n by

$$n(t) = g\int \frac{d^3p}{(2\pi)^3} f, \tag{C.3}$$

where g is the species degrees of freedom describing the degeneracy of the particle. For example, the g of a quark has two spin states, three colour states, and two states per generation $g_q = 2\times 3\times 2 = 12$. We can substitute the Louville operator and integrate by parts

$$\dot{n} + 3Hn = \frac{g}{(2\pi)^3}\int C[f]\frac{d^3p}{E}, \tag{C.4}$$

where the Hubble constant $H = \dot{a}/a$. Note that if collisional contribution to the change of number density is zero, i.e., $C[f] = 0$, the equation says that na^3 is a constant agreeing with our intuition. The collisional contribution is more involved and depends on the kinematic of the scattering process. For our work, we consider only the tree level $2 \leftrightarrow 2$ process $\chi\bar{\chi} \leftrightarrow X\bar{X}$, which for one species of DM

$$\begin{aligned} g_\chi \int C[f_\chi]\frac{d^3p_1}{(2\pi)^3} = -\sum_{spins}\int & d^4\Pi(2\pi)^4[f_\chi f_{\bar{\chi}}(1\pm f_X)(1\pm f_{\bar{X}})|M_{\chi\bar{\chi}\to X\bar{X}}|^2 \\ & - f_X f_{\bar{X}}(1\pm f_\chi)(1\pm f_{\bar{\chi}})|M_{X\bar{X}\to\chi\bar{\chi}}|^2]\delta^4(p_\chi + p_{\bar{\chi}} - p_X - p_{\bar{X}}). \end{aligned} \tag{C.5}$$

We absorbed all the phase space scaling terms to $d\Pi_i = d^3p_i/(2\pi)^3 2E_i$, and g_χ is the species degree of freedom of particle χ. For the purpose of our discussion, we follow a standard derivation [22, 23] by assuming time reversal invariance (equivalently CP), so that the scattering matrix elements are identical $|M_{\chi\bar{\chi}\to X\bar{X}}|^2 = |M_{X\bar{X}\to\chi\bar{\chi}}|^2$. We can assume the SM species are in thermal equilibrium at all times to simplify the integrand with Boltzmann distribution. The factors $1\pm f$ represent Einstein-Boseman or Fermi-Dirac statistics, where the plus signs allow co-occupation and the minus sign punishes fermions occupying the same state. We assume that the energy of the particles are high enough that there is no condensation/degeneracy because $T_i \ll E_i - \mu_i$. This approximates $1\pm f \approx 1$ leading us to

$$\dot{n}_\chi + 3Hn_\chi = -\sum_{spins}\int d^4\Pi|M|^2(f_\chi f_{\bar{\chi}} - f_X f_{\bar{X}})(2\pi)^4\delta^4(p_\chi + p_{\bar{\chi}} - p_X - p_{\bar{X}}). \tag{C.6}$$

The left-hand side is the covariant change calculated earlier, and the delta function enforces momentum and energy conservation before and after the scattering. Also, we can use Boltzmann distribution since the SM particles are in thermal equilibrium with the universe

$$f_X = \exp(-E_X/T), \quad f_{\bar{X}} = \exp(-E_{\bar{X}}/T), \tag{C.7}$$

assuming negligible chemical potential. Once the DM reaches thermal equilibrium, it would have the same Boltzmann distribution in the phase space,

$$f_X f_{\bar{X}} = \exp[-(E_X + E_{\bar{X}})/T] = \exp[-(E_\chi + E_{\bar{\chi}})/T] = f_\chi^{eq} f_{\bar{\chi}}^{eq}. \tag{C.8}$$

The matrix element integral can be found through standard definition [22]

$$\begin{aligned}&\sum_{spin} \int |M|^2 (2\pi)^4 \delta^4(p_\chi + p_{\bar{\chi}} - p_X - p_{\bar{X}}) d\Pi_X \Pi_{\bar{X}} \\ &\quad = 4 g_\chi g_{\bar{\chi}} \sigma_{\chi\bar{\chi}} \sqrt{(p_\chi \cdot p_{\bar{\chi}})^2 - (m_\chi \cdot m_{\bar{\chi}})^2},\end{aligned} \tag{C.9}$$

Substituting everything leads to a dynamical equation for the number density of the DM in terms of its equilibrium density, using the definition for the Møller velocity $v_{\chi\bar{\chi}} = \sqrt{(p_\chi \cdot p_{\bar{\chi}})^2 - (m_\chi \cdot m_{\bar{\chi}})^2}/E_\chi E_{\bar{\chi}}$ [22, 24, 39]

$$\dot{n}_\chi + 3Hn_\chi = \langle \sigma v_{\chi\bar{\chi}} \rangle (n_{eq}^2 - n_\chi^2), \tag{C.10}$$

and the angled bracket represents thermal average of the incoming momentum. From this point on, we will drop the subscripts since we are interested in one species of DM. Using normalised number density $Y = n/s$ and the constant property of overall entropy $d(sa^3)/dt = 0$ reduces equation (C.10)

$$\dot{Y} = s \langle \sigma v \rangle (Y_{eq}^2 - Y^2). \tag{C.11}$$

The universe cools as it expands because it is confined in a "box" of the expansion length scale a, which limits the longest wavelength. The temperature is inversely proportional to the expansion scale $T \propto 1/a$ and makes T a good measure of time. We use rescaled time $x = m/T$ to be the independent variable. Using $H = \dot{a}/a$ we can derive $\dot{x} = xH$ and the dynamic equation (C.11) becomes the following

$$\frac{dY}{dx} = \frac{s\langle \sigma v \rangle}{xH} (Y_{eq}^2 - Y^2). \tag{C.12}$$

Therefore, we found the dynamical equation that governs the evolution of the DM independent of the physics behind DM itself. The only assumption we made was that the scattering with SM particle is a $2 \leftrightarrow 2$ process, and the cross section $\langle \sigma v \rangle$ contains all the physics behind DM scattering.

C.2 Decoupling and freeze-out

At first, the DM density is so high that its density evolution is the same as the equilibrium up to a point x_f,

$$Y(x < x_f) \approx Y_{eq}(x). \tag{C.13}$$

After time scale x_f, the inelastic scattering rate loses to the Hubble expansion H. Once the density dilutes so much that DM cannot find one another to annihilate, it decouples from SM particles and the inelastic scattering ceases. The DM density therefore remains constant after a *freeze out time* x_f

$$Y(x > x_f) \approx Y_{eq}(x_f). \tag{C.14}$$

If the freeze out happen early, the DM would still be relativistic or *hot*, after it decouples and stay that way. On the other end of the spectrum, the DM is *cold* if it is non-relativistic after freeze out. The cold DM density in equilibrium is derived in Kolb and Turner [23]

$$Y_{\text{eq}} = 0.145 \frac{g}{g_* s} x^{3/2} e^{-x}, \tag{C.15}$$

where $g_* s$ contains information about the dominating particle contents of the universe and at present day $g_* s \approx 3.91$. [3]

$$g_* s = \sum_{\text{boson}} g_i (T_i/T)^3 + \frac{7}{8} \sum_{\text{fermion}} g_i (T_i/T)^3. \tag{C.16}$$

This means that after the freeze out, the equilibrium solution decays exponentially and is therefore negligible compared to the relic. Equation (C.12) approximates

$$\frac{dY}{dx} \approx -\frac{s_0 \langle \sigma v \rangle_0}{x^2 H} Y^2, \tag{C.17}$$

where we extracted the entropy dependence $s = s_0 x^{-3}$ and $\langle \sigma v \rangle = \langle \sigma v \rangle_0 x^{-n}$ setting $n = 0$ because the thermal averaging expanded around the relativistic limit $\langle \sigma v \rangle \sim b_0 + b_1 x^{-1}$, where $b_0 = \langle \sigma v \rangle_0$ dominates if non-relativistic. We can integrate (C.17) from the freeze out time x_f to infinity

$$Y_{\text{today}} \approx \frac{x_f H}{s_0 \langle \sigma v \rangle_0}. \tag{C.18}$$

Crucially, we can calculate the observable fraction of critical density ρ_c contributed by DM

$$\Omega_\chi h^2 \propto \left[\int_{x_f}^{\infty} \frac{\langle \sigma v \rangle}{x^2} dx \right]^{-1} \approx \frac{m s_{\text{today}} Y_{\text{today}}}{\rho_c}, \tag{C.19}$$

and substitute in (C.18)

$$\Omega h^2 = \frac{1.07 \times 10^9 x_f}{g_*^{1/2} M_{PL} \langle \sigma v \rangle}, \tag{C.20}$$

where M_{PL} is the Planck mass. We can use this to constrain the parameter space independent of the UV theories behind DM. If we know $\langle \sigma v \rangle$, we can calculate the freeze-out time x_f [23]

$$x_f \approx \ln[0.038 (g_* x_f)^{-1/2} M_{PL} m_s \langle \sigma v \rangle], \tag{C.21}$$

which is all we need to know to relate the relic density of a particle's decoupling to the cross section.

[3] In present day $T/T_\nu = (11/4)^{1/3}$, so summing over every species $g_* s = 2 + \frac{7}{8} \times 2 \times 3 \times \frac{4}{11} = 3.91$

C.3 Thermal average cross section

The thermal average of the scattering cross section relies on the assumption that the produced particles are in thermal equilibrium with the rest of the universe, so the produced particles are individually a canonical ensemble of the universal reservoir. We can therefore write down the thermal average using the Boltzmann distribution

$$\langle \sigma v \rangle = \frac{\int \sigma v dn_\chi^{eq} dn_{\bar{\chi}}^{eq}}{\int dn_\chi^{eq} dn_{\bar{\chi}}^{eq}} = \frac{\int \sigma v e^{-E_\chi/T} e^{-E_{\bar{\chi}}/T} d^3p_\chi d^3p_{\bar{\chi}}}{\int e^{-E_\chi/T} e^{-E_{\bar{\chi}}/T} d^3p_\chi d^3p_{\bar{\chi}}}, \tag{C.22}$$

assuming Maxwell-Boltzmann statistics. Velocity used here is the Møller velocity, which is the relativistic relative velocity independent of frame and dervied by considering the relativistic flux, which reduces to the centre of mass frame velocity in the non-relativistic limit [24]

$$\langle \sigma v_{\text{Møl}} \rangle = \langle \sigma v \rangle_{\text{lab}} = \frac{1}{2}\left[1 + \frac{K_1^2(x)}{K_2^2(x)}\right] \langle \sigma v \rangle_{\text{CoM}}, \tag{C.23}$$

where K_i are 2nd order Bessel functions, and in the non-relativistic limit $x \longrightarrow \infty$, the three quantities are identical. We can parameterise integral (C.22) in spherical coordinate, and without the loss of generality, set one of the momentum vector to align with the axis

$$d^3p_\chi d^3p_{\bar{\chi}} = 4\pi p_\chi dE_\chi \cdot 4\pi p_{\bar{\chi}} dE_{\bar{\chi}} \cdot d(cos\theta)/2, \tag{C.24}$$

where θ is the angle subtended by the two momentum vectors. We can instead integrate over $s = 2m^2 + 2E_\chi E_{\bar{\chi}} - 2p_\chi p_{\bar{\chi}} cos\theta$ through a change of variable and find that [24]

$$\int_\Omega \sigma v \cdot e^{-E_\chi/T} e^{-E_{\bar{\chi}}/T} d^3p_\chi d^3p_{\bar{\chi}} = \pi^2 T \int_{4m^2}^{\infty} \sigma v \cdot s\sqrt{s - 4m^2} K_1(\sqrt{s}/T) ds \tag{C.25}$$

The normalisation factor can similarly be calculated

$$\int e^{-E_\chi/T} e^{-E_{\bar{\chi}}/T} d^3p_\chi d^3p_{\bar{\chi}} = [4\pi m^2 T K_2(m_s/T)]^2, \tag{C.26}$$

and the thermally averaged cross section is therefore

$$\langle \sigma v \rangle = \frac{\int_{4m^2}^{\infty} \sigma v \cdot s\sqrt{s - 4m_s^2} K_1(\sqrt{s}/T) ds}{16 T m_s^4 K_2^2(m_s/T)}, \tag{C.27}$$

and equals to the following expressed in normalised time $x = m_s/T$

$$\langle \sigma v \rangle = \frac{x}{16 m_s^5 K_2^2(x)} \int_{4m^2}^{\infty} \sigma v \cdot s\sqrt{s - 4m^2} K_1(\sqrt{s}/T) ds, \tag{C.28}$$

References

[1] Vera C. Rubin and Jr. Ford, W. Kent. Rotation of the Andromeda Nebula from a Spectroscopic Survey of Emission Regions. , 159:379, February 1970.

[2] Niels C.M. Martens and Dennis Lehmkuhl. Dark matter = modified gravity? scrutinising the spacetime–matter distinction through the modified gravity/ dark matter lens. *Studies in History and Philosophy of Science Part B: Studies in History and Philosophy of Modern Physics*, 72:237–250, 2020.

[3] M. Milgrom. A modification of the Newtonian dynamics as a possible alternative to the hidden mass hypothesis. , 270:365–370, July 1983.

[4] Timothy Clifton, Pedro G. Ferreira, Antonio Padilla, and Constantinos Skordis. Modified gravity and cosmology. *Physics Reports*, 513(1):1–189, 2012. Modified Gravity and Cosmology.

[5] Sacha Davidson, Paolo Gambino, Mikko Laine, Matthias Neubert, and Christophe Salomon. *Effective Field Theory in Particle Physics and Cosmology: Lecture Notes of the Les Houches Summer School: Volume 108, July 2017*. Oxford University Press, 04 2020.

[6] S. Coleman, J. Wess, and Bruno Zumino. Structure of phenomenological lagrangians. i. *Phys. Rev.*, 177:2239–2247, Jan 1969.

[7] Curtis G. Callan, Sidney Coleman, J. Wess, and Bruno Zumino. Structure of phenomenological lagrangians. ii. *Phys. Rev.*, 177:2247–2250, Jan 1969.

[8] Timothy Cohen, Nathaniel Craig, Xiaochuan Lu, and Dave Sutherland. Is SMEFT enough? *Journal of High Energy Physics*, 2021(3), mar 2021.

[9] Ian Banta, Timothy Cohen, Nathaniel Craig, Xiaochuan Lu, and Dave Sutherland. Non-decoupling new particles. *Journal of High Energy Physics*, 2022(2), feb 2022.

[10] Rodrigo Alonso, Elizabeth E. Jenkins, and Aneesh V. Manohar. Geometry of the scalar sector. *Journal of High Energy Physics*, 2016(8), aug 2016.

[11] Rodrigo Alonso, Elizabeth E. Jenkins, and Aneesh V. Manohar. A geometric formulation of higgs effective field theory: Measuring the curvature of scalar field space. *Physics Letters B*, 754:335–342, 2016.

[12] Timothy Cohen, Nathaniel Craig, Xiaochuan Lu, and Dave Sutherland. Unitarity violation and the geometry of higgs EFTs. *Journal of High Energy Physics*, 2021(12), dec 2021.

[13] Steven Weinberg. On the development of effective field theory. *The European Physical Journal H*, 46(1), mar 2021.

[14] Timothy Cohen, John Kearney, Aaron Pierce, and David Tucker-Smith. Singlet-doublet dark matter. *Phys. Rev. D*, 85:075003, Apr 2012.

[15] ATLAS Collaboration. A detailed map of higgs boson interactions by the ATLAS experiment ten years after the discovery. *Nature*, 607(7917):52–59, jul 2022.

[16] CMS Collaboration. Combined measurements of higgs boson couplings in proton-proton collisions at $\sqrt{s}$= 13 tev. *The European Physical Journal C*, 79(5), may 2019.

[17] ATLAS Collaboration. Combined measurements of higgs boson production and decay using up to 80fb^{-1} of proton-proton collision data at $\sqrt{s}$= 13 tev collected with the atlas experiment. *Physical Review D*, 101(1), jan 2020.

[18] Alexander Belyaev, Giacomo Cacciapaglia, Igor P. Ivanov, Felipe Rojas-Abatte, and Marc Thomas. Anatomy of the inert two-higgs-doublet model in the light of the lhc and non-lhc dark matter searches. *Phys. Rev. D*, 97:035011, Feb 2018.

[19] Amalia Betancur, Guillermo Palacio, and Andrés Rivera. Inert doublet as multicomponent dark matter. *Nuclear Physics B*, 962:115276, 2021.

[20] Nilendra G. Deshpande and Ernest Ma. Pattern of symmetry breaking with two higgs doublets. *Phys. Rev. D*, 18:2574–2576, Oct 1978.

[21] Aleph, Delphi, L3, OPAL Collaborations, and the LEP working group for Higgs boson searches. Search for charged higgs bosons: Combined results using lep data, 2013.

[22] Mariangela Lisanti. Lectures on dark matter physics. In *New Frontiers in Fields and Strings*. WORLD SCIENTIFIC, nov 2016.

[23] Edward W. Kolb and Michael S. Turner. *The Early Universe*, volume 69. 1990.

[24] Paolo Gondolo and Graciela Gelmini. Cosmic abundances of stable particles: Improved analysis. *Nuclear Physics B*, 360(1):145–179, 1991.

[25] James D. Wells. Annihilation cross sections for relic densities in the low velocity limit, 1994.

[26] Planck Collaboration. Planck 2018 results - vi. cosmological parameters. *A&A*, 641:A6, 2020.

[27] Jonathan Cornell and. Global fits of scalar singlet dark matter with GAMBIT. In *Proceedings of 38th International Conference on High Energy Physics — PoS(ICHEP2016)*. Sissa Medialab, feb 2017.

[28] Mark Thomson. *Modern particle physics / Mark Thomson (University of Cambridge).* 2013.

[29] XENON Collaboration. First dark matter search with nuclear recoils from the xenonnt experiment, 2023.

[30] C.P. Burgess, Maxim Pospelov, and Tonnis ter Veldhuis. The minimal model of nonbaryonic dark matter: a singlet scalar. *Nuclear Physics B*, 619(1-3):709–728, dec 2001.

[31] ATLAS collaboration. Measurements of the higgs boson production and decay rates and coupling strengths using pp collision data at $\sqrt{s} = 7$ and 8 TeV in the ATLAS experiment. *The European Physical Journal C*, 76(1), jan 2016.

[32] Peter Athron, , Csaba Balázs, Torsten Bringmann, Andy Buckley, Marcin Chrząszcz, Jan Conrad, Jonathan M. Cornell, Lars A. Dal, Joakim Edsjö, Ben Farmer, Paul Jackson, Felix Kahlhoefer, Abram Krislock, Anders Kvellestad, James McKay, Farvah Mahmoudi, Gregory D. Martinez, Antje Putze, Are Raklev, Christopher Rogan, Aldo Saavedra, Christopher Savage, Pat Scott, Nicola Serra, Christoph Weniger, and Martin White. Status of the scalar singlet dark matter model. *The European Physical Journal C*, 77(8), aug 2017.

[33] Ankit Beniwal. Global Fits of Dirac Dark Matter Effective Field Theories. In *14th International Workshop on the Identification of Dark Matter 2022*, 10 2022.

[34] Christopher Chang, Pat Scott, Tomás E. Gonzalo, Felix Kahlhoefer, Anders Kvellestad, and Martin White. Global fits of simplified models for dark matter with gambit i. scalar and fermionic models with s-channel vector mediators, 2022.

[35] Christopher Chang, Pat Scott, Tomás E. Gonzalo, Felix Kahlhoefer, and Martin White. Global fits of simplified models for dark matter with gambit ii. vector dark matter with an s-channel vector mediator, 2023.

[36] Nathaniel Craig, Hou Keong Lou, Matthew McCullough, and Arun Thalapillil. The higgs portal above threshold, 2014.

[37] James M. Cline, Pat Scott, Kimmo Kainulainen, and Christoph Weniger. Update on scalar singlet dark matter. *Physical Review D*, 88(5), sep 2013.

[38] Ian Banta, Timothy Cohen, Nathaniel Craig, Xiaochuan Lu, and Dave Sutherland. Effective Field Theory of the Two Higgs Doublet Model. 4 2023.

[39] Kim Griest and David Seckel. Three exceptions in the calculation of relic abundances. *Phys. Rev. D*, 43:3191–3203, May 1991.